Journal of Thermal Analysis and Calorimetry (2024) 149:9575–9586
https://doi.org/10.1007/s10973-024-13453-5

Size scale effect on mass burning flux and flame behavior of solid fuels

Peiyi Sun[1] · Tianhang Zhang[1] · Xinyan Huang[1]

Received: 26 October 2023 / Accepted: 8 July 2024 / Published online: 20 August 2024
© The Author(s) 2024

Abstract

The study investigates the horizontal fuel size effect on free-burning fires for PMMA plates and wood cribs. The fuel size effect on mass burning flux and flame behavior is mainly discussed and compared with typical pool fires. For the PMMA plate and liquid pool, when the fuel size is small (< 10 cm), either the 3D sidewall burning of PMMA or the container wall heated by flame can promote the burning flux at the horizontal projection area. As the fuel size increases, these side wall burning or heating effects decrease, causing the drop in burning flux with fuel scale for both the PMMA plate and liquid pool. For small-scale wood cribs, fire cannot self-sustain due to the large airflow cooling. With the increase in wood crib size, the burning rate first remains constant and then gradually increases, driven by the enhanced internal radiation. As the fuel size increases above 20–30 cm, the flame radiation dominates the burning flux for all fuel types. Fire dynamics simulator (FDS) was adopted to simulate the horizontal size effect by setting a varied fire source (horizontal projection) area. First, the flame geometry and heat release rate (HRR) of simulations were validated against experimental results. Subsequently, the validated fire model generates cases covering a broad range of fire scales. Finally, a new correlation of flame height with the fire heat release rate and fuel size is proposed, and its prediction capability is validated in the numerical fire modeling. This study quantifies the size effect on the burning rate for common solid fuels and provides valuable information for the numerical modeling of multi-scale fires.

Keywords Burning flux · Wood cribs · Flame height · Heat release rate · Numerical validation

Abbreviations

FDS	Fire dynamics simulator
HRR	Heat release rate
HRRPUA	Heat release rate per unit area
LES	Large eddy simulation
PMMA	Polymethyl methacrylate
2D	Two dimensional
3D	Three dimensional

List of symbols

A_h	Horizontal projection area (m^2)
A_s	Exposed surface area (m^2)
A_v	Area of the vertical crib shafts (m^2)
b	Length of the wood strip (m)
D	Fuel bed diameter (m)
D_c	Critical fuel bed diameter (m)
Δh_{evp}	Heat of evaporation ($kJ \cdot kg^{-1}$)
Δh_{py}	Heat of pyrolysis ($kJ \cdot kg^{-1}$)
l	Flame height (m)
L^*	Dimensionless flame height (–)
$\dot{m}''$	Mass loss flux ($g \cdot m^{-2} \cdot s^{-1}$)
N	The layer of the wood crib (–)
$\dot{q}''$	Heat flux ($kW \cdot m^{-2}$)
$\dot{Q}_c$	Convective heat release rate (kW)
t	Time (s)
T	Temperature (°C)

Greeks

δ	Thickness of fuel (m)
Φ	Porosity factor (–)

Subscripts

c	Critical
cond	Conduction
h	Horizontal projection area
s	Surface area
v	Vertical crib shafts
0	Initial

✉ Tianhang Zhang
tianhang.zhang@connect.polyu.hk

✉ Xinyan Huang
xy.huang@polyu.edu.hk

[1] Research Centre for Smart Urban Resilience and Firefighting, Department of Building Environment and Energy Engineering, The Hong Kong Polytechnic University, Kowloon, Hong Kong, China

Introduction

Mass burning rate is the critical parameter to evaluate the consumption of fuels within flame boundaries [1]. Generally, the burning rate indicates the mass loss rate in the condensed phase, either through the evaporation of liquid fuel or through the pyrolysis of solid fuel [2]. It is essential for determining flame height, heat release rate, and fire sizes [3]. The burning rate also depends upon the energy feedback from the flame to the heating zone beneath the flame [4]. The feedback loop is coupled between the condensed and gas phases, dominating the fire development. By studying the mass burning rate of different materials in different scales, it provides fundamental knowledge in quantifying and predicting the fire risks in complex fire scenarios.

The burning rate of various fuels has been investigated, typically including liquid fuels [5–7], plastics [8, 9], and wood cribs [10, 11]. Liquid pool fire behavior is relatively simple and easy to control compared with the above-mentioned solid fuels. Therefore, pool fire was widely adopted in different fire test scenarios, e.g., compartment fire [12], tunnel fire [13], and structural fire [14]. During the past decades, the effects of pool scale [15], ambient boundary [16], ground temperature [17], and external wind and pressure [18, 19] were well studied. Among those parameters, the pool size is considered to be the most important factor to characterize the liquid pool fire burning rate in natural ventilation conditions [20]: With the increase in pool scale, the burning rate first decreases in a laminar flow regime and then increases continuously up to a maximum value and remains constant when reaching the fully turbulent regime [21].

In general, the solid fuel has two types: non-charring and charring. The non-charring materials burned completely with no residue, which can be modeled using a similar theory with flammable liquids. Many studies investigate the burning of polymethyl methacrylate (PMMA) in different scales and with or without additional radiation heat flux. Gollner et al. [22] found that flame radiation dominated the burning rate of a 10×20 cm^2 flat PMMA plate. Zhu et al. [23] found that it took up to 20 min for a flame spread and burning of a 4-mm PMMA plate to reach the steady state Steckler et al. [24] presented an analytical model for the transient gasification of a non-charring thermoplastic material exposed to an external heat flux in a nitrogen atmosphere, which only considers the non-flaming scenario. Modak and Croce [25] studied the burning behavior of PMMA plate fires of different sizes in both laminar and turbulent conditions. They discovered that flame radiation significantly impacted the burning rate, particularly for turbulent fires. Kacem et al. [26] burned the horizontally oriented PMMA slabs in the open air with side lengths of 10 cm, 20 cm, and 40 cm. They concluded that the radiative heat transfer increased with sample size, but its ratio remained constant (around 80%). However, the above tests of PMMA plates eliminate the flame heat feedback at edges by covering or blocking the side walls. In real fire scenarios, the flame can cover the entire free surface of the fuel in contact with air. Therefore, more studies are needed to evaluate the scale effect on free-burning solid fuel.

The modeling of the crib fire behavior is more complex and involved more parameters, e.g., porosity, dimension, ignition, and so on. The study on wood crib fire has a long history of about 90 years, with early available data from 1937 [27]. Gross [28] demonstrated that the burning rate of unconfined cribs occurs in two regimes: open (or loosely packed) and closed (or densely packed), representing two states of the crib burning behavior, respectively: 1) The natural limit of strip surfaces burning freely and the fire heat release rate are controlled by the flame spread between each strip; 2) for a tightly packed crib, the burning rate is controlled by the maximum air flow rate through the air holes in the crib [29]. The porosity factor, considering the clear spacing, strip thickness, and crib height, was adopted to quantify the different fire behaviors [28]. Unfortunately, limited studies discussed the horizontal size effect on the crib fire. Overall, the scale effect, including the correlation and mechanism, for the liquid pool fire is already clear. However, there is a noticeable lack of studies discussing the scale effect of solid fuels, both in plate and in crib configurations. Furthermore, a systematic exploration of the factors influencing burning flux for different solid fuels is yet to be undertaken.

In the current study, a series of free-burning tests are performed to determine the burning rate of PMMA plates and wood cribs with varied small scales. The peak burning flux and flame behavior have been mainly analyzed and compared with liquid fuels. Then, the equivalence of heat release rate per unit area (HRRPUA) in the burning of different fuel types is also discussed. Finally, a new correlation of flame height with the fire heat release rate and fuel size is proposed, and its prediction capability is validated. This study provides insight into underlying dominating factors affecting the burning rate of different fuel types at different sizes and provides valuable data for fire safety evaluation.

Experimental

To study the scale effect of solid fuels, a series of burning tests were conducted with different fuel types and sizes. The mass data during the burning process are measured by an electric balance with an accuracy of 0.1 g and 0.1s time intervals. The mass loss was adopted to calculate the fire heat release rate subsequently. The flame behavior is recorded with a video camera to analyze the flame height (Fig. 1a). PMMA plate and wood crib are selected as typical

solid fuels. The thermoset PMMA plate was pre-cut into five sizes. Noted that the fuel size is varied in the horizontal direction and the fuel thickness is consistent for a fair comparison. In detail, the side length of the PMMA plate ranges from 5 to 30 cm with the same thickness of 2 cm (Fig. 1b, c). A heating panel was utilized to pre-heat the PMMA plate surface to reach 350 °C before the test to avoid uneven ignition. Then, the flame could easily be triggered by applying a lighter.

For the wood strip, the cross-section is a square with 2.5 cm side length, and the length ranges from 5 to 40 cm (Fig. 1b). Along the horizontal dimension, the length/width of the wood crib ranges from 5 to 40 cm; and along the vertical dimension, the height ranges from 10 to 20 cm. The clear spacing is fixed as 2.5 cm (Fig. 1c). Thirty milliliter propanol is used to ignite the wood crib for all cases. Besides, a set of liquid fuel (propanol) burning tests with pool diameters ranging from 9 to 29 cm are also carried out for better comparison. The thickness of the liquid fuel is fixed at 2 cm. Detailed test conditions are summarized in Table 1. Duplicated tests were conducted for each case to analyze the random uncertainty.

In this study, the flame height data are acquired by a set of image processing algorithms. The original RGB images are first converted to a binary image. Then the binary values of the image sequences that contain 25 continuous frames (one second) are averaged by time in each pixel, as demonstrated in Fig. 2. The timeaveraged gray images essentially represent the occurrence frequency of the flame in each pixel. Zukoski et al. [30] defined the mean flame height as the height at which the flame appears half the time, i.e., at which the intermittency is 0.5. Therefore, a threshold of 0.5 is adopted to determine the flame zone and background zone, respectively. By analyzing the coordinate distribution of flame region pixels, the pixel length occupied by the flame in the vertical direction can be determined. Subsequently, by comparing the pixel length with a known reference length present in the image, the height of the flame can be obtained. By employing this method, a more stable distribution of flame heights can be achieved, while effectively mitigating the impact of background items, turbulent fluctuation, and firebrands.

Results and discussion

Burning process and fire phenomenon

The burning process consists of three stages: ignition, development, and decay. Liquid pools can be easily ignited with a pilot source, while PMMA and wood cribs require pre-heating. Figure 3 presents the free-burning process of PMMA plates at small and large scales. As the top surface of the PMMA sample was pre-heated to the pyrolysis temperature (~ 400 °C), the flame can quickly develop and cover the entire top surface. It then spreads downward along the sidewall and finally engulfs the entire fuel (Fig. 3a). In particular, the regression process exhibits different behavior for PMMA at different scales. Small-scale PMMA has a more pronounced horizontal regression than vertical regression. Nevertheless, large-scale PMMA

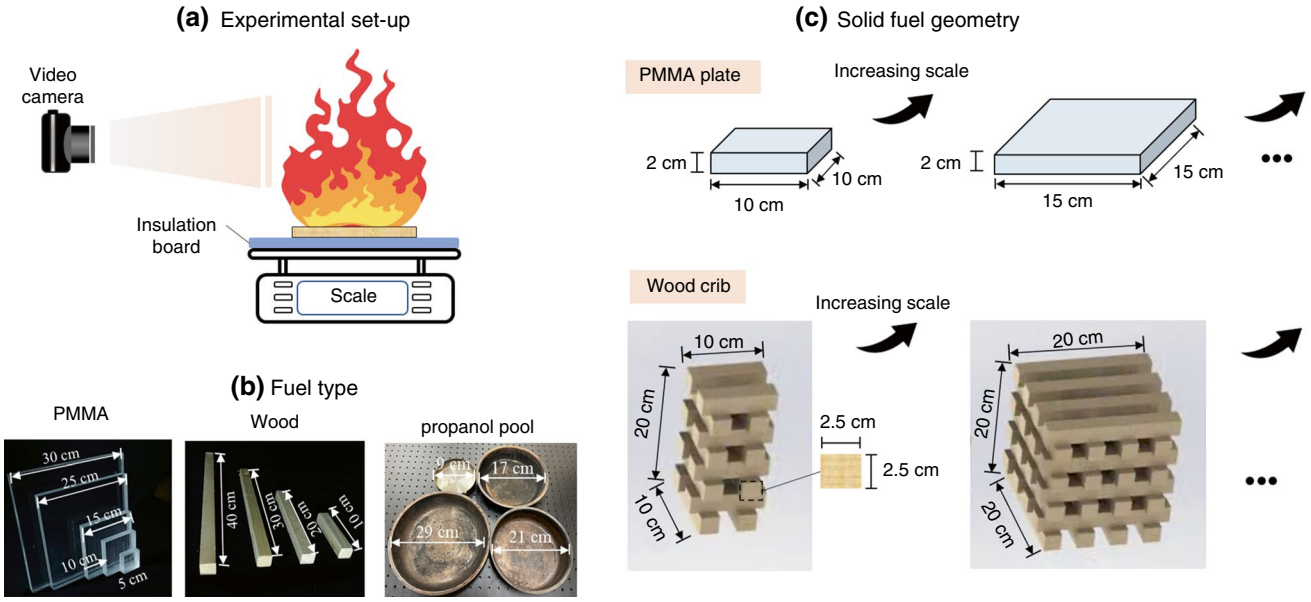

Fig. 1 Experimental setup and fuel geometry

Table 1 Summary of all test conditions, where case no. is named by fuel-length-height. P, W, and L represent PMMA, wood crib, and liquid pool fire, respectively; the porosity factor of the wood crib is calculated with $\Phi = N^{1/2}b^{1.1}\left(A_v/A_s\right)$ [28], where N is the layer of the wood crib, b is the length of the wood strip cross-section, and A_s and A_v are the exposed surface area and total cross-sectional area of the vertical crib shafts, respectively

Fuel type	Case No.	Side length/ cm	Height or thickness/ cm	Surface-to-volume ratio/ cm^{-1}	Porosity factor
PMMA	P-5-2	5	2	1.3	/
	P-10-2	10		0.9	
	P-15-2	15		0.77	
	P-20-2	20		0.7	
	P-25-2	25		0.66	
	P-30-2	30		0.63	
Wood crib	W-5-20	5	20	0.91	0.027
	W-10-20	10		0.81	0.030
	W-20-20	20		0.76	0.032
	W-30-20	30		0.75	0.032
	W-40-20	40		0.74	0.033
	W-20-10	20	10	0.77	0.036
	W-20–15	20	15	0.78	0.044
Liquid (propanol)	L-9-2	9	2	0.5	/
	L-12-2	12		0.5	
	L-21-2	21		0.5	
	L-29-2	29		0.5	

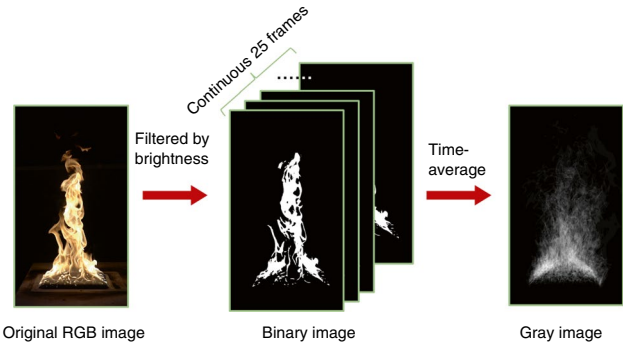

Fig. 2 Image processing to identify the flame height

regresses mainly in the vertical direction, and the center part of the fuel burns out first (Fig. 3b).

Figure 4 compares the typical flame patterns of PMMA and wood crib fires in varied scales. The flame was captured when the burning entranced an intensive burning stage so that the flame fully covered the fuel. As the fire size increased, the flame became more turbulent, and the flame height increased. The wood crib was ignited by an ethanol pool fire at the bottom, which first ignited the center wood strips and spread to the edges. Once the wood was ignited, the firebrands were observed, and larger wood cribs fire showed more intensive firebrands. The flame is more difficult to sustain on wood cribs with larger porosity (small size) or fewer layers (small thickness). In a case with self-sustained flame, wood strips can burn out into ash in the end.

Burning mass rate

The mass loss flux is calculated using the mass loss rate divided by the horizontal projection area (A_h) of the fuel. Although the real burning area is a curved surface in three dimensions and is changed with the regression of the fuel in the horizontal direction, a constant burning area is assumed to simplify the evaluation of the burning flux for all three types of fuels. The average mass loss rate during the period of the maximum burning stage is selected as the representative burning rate. Since the entire burning duration of the PMMA and propanol pool (over 20 min) is doubled than that of the wood crib (less than 10 min), a 5-min time interval is adopted to measure the peak burning flux for PMMA and propanol pool, and the 2-min interval is used for wood cribs.

The mass flux evolution trend of the PMMA plate in three sizes is shown in Fig. 5a. The small PMMA size reaches the peak value faster than large scales. In particular, the mass loss flux gradually decreases after reaching the peak value for small-scale PMMA (10 cm). Note that the mass flux has been underestimated in the late burning stage because the real flame area decreases with the regression fuel area in the horizontal direction, but the horizontal regression is not obvious for large-scale PMMA as described above. Nevertheless, this underestimation does not affect the peak value that is focused on in this study. As the scale increases, the intensive burning stage lasts longer. The middle-scale PMMA even maintains a nearly constant burning rate. The large-scale PMMA shows a continuously increased burning flux, with the peak value

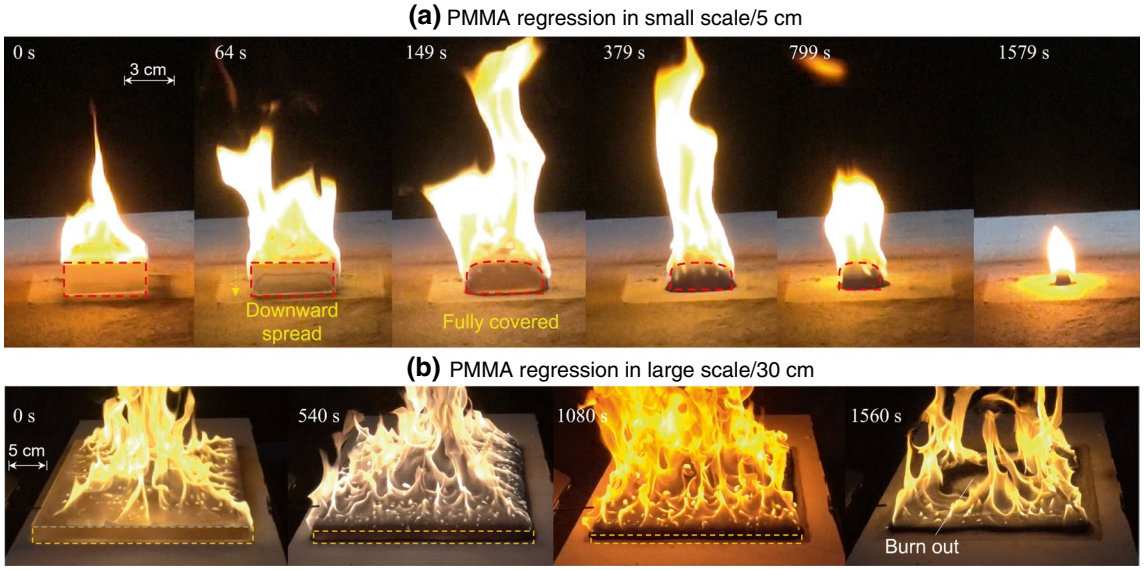

Fig. 3 Burning and regression process of PMMA slab with **a** small and **b** large horizontal projection area

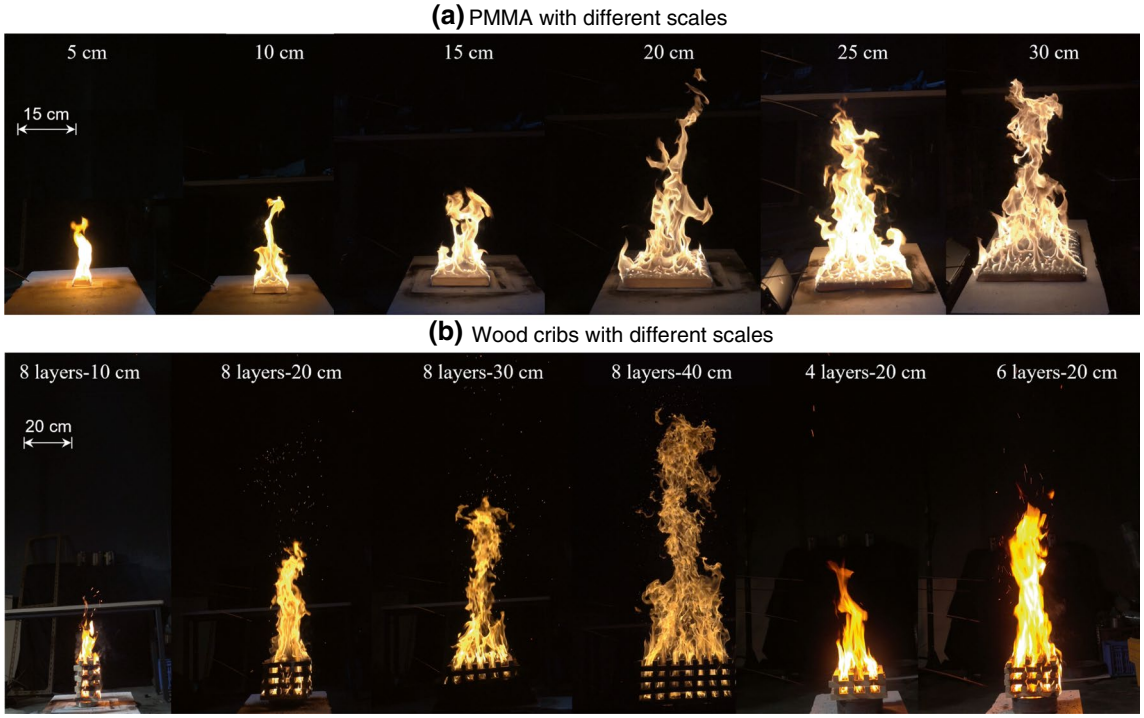

Fig. 4 Flame shape of solid fuel in fully developed stage **a** PMMA plate and **b** wood cribs with different horizontal projection area and layer numbers

appearing in the late burning stage. Finally, the burning flux drops because of the burnout of fuel.

Figure 5b presents the burning flux of the propanol pool with varied diameters. The data were processed similarly to PMMA, where the averaged burning flux around the peak value was selected for analysis. In general, large-scale pool fire has a higher burning flux. Since the initial fuel thickness remains constant (2 cm) for all pool sizes, the total burning time is decided by the burning flux for each scale.

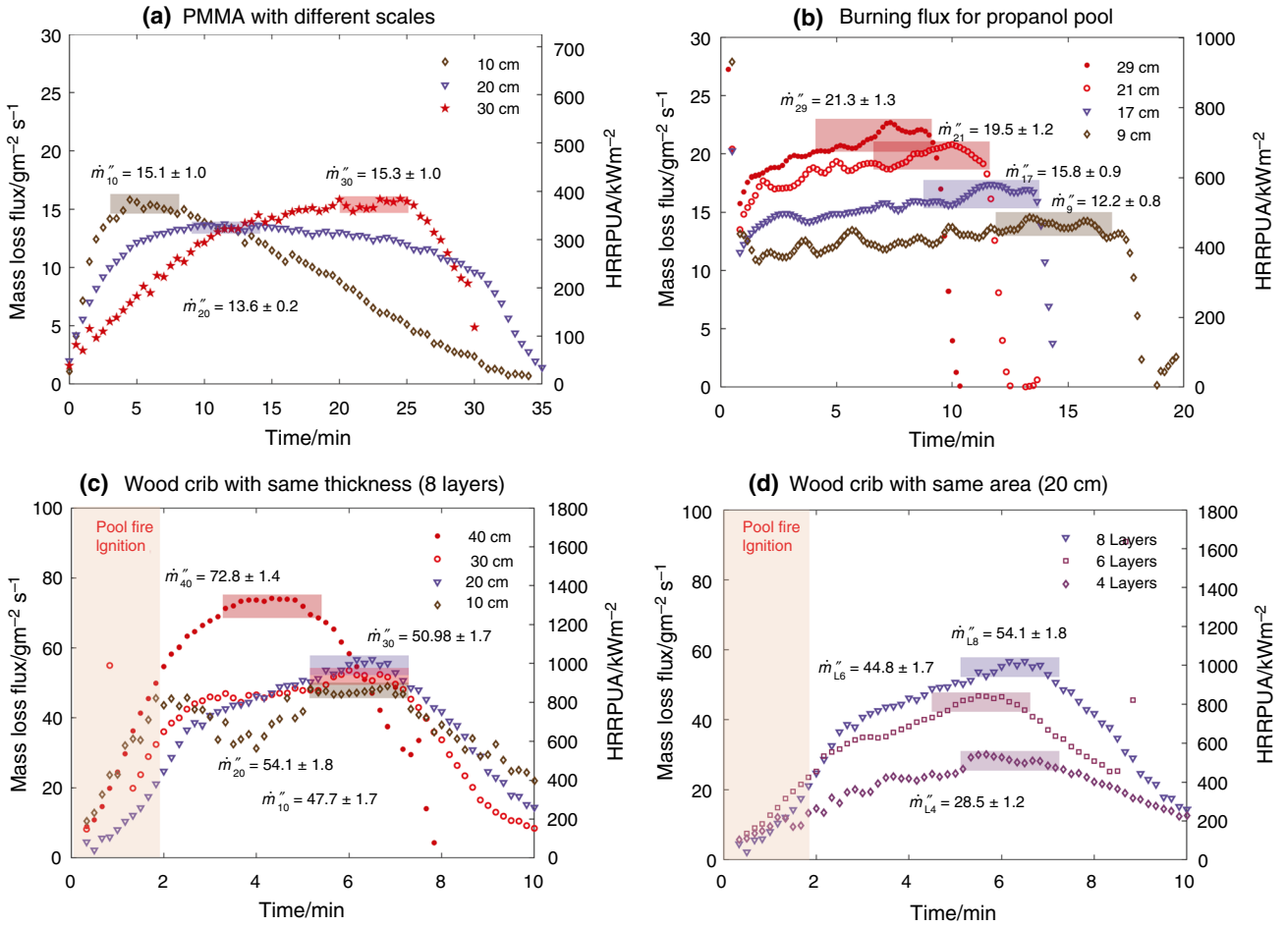

Fig. 5 Transient mass loss flux and HRRPUA with scale effect, **a** PMMA plate, **b** propanol pool, **c** wood cribs (eight layers), and **d** wood cribs with different layer numbers

As a result, the pool fire with a smaller diameter has longer burning durations.

The burning of the wood crib is more complex than PMMA and liquid fuels. Figure 5c and d presents the scale effects in varied top surface areas and thicknesses. The wood cribs were ignited by an ethanol pool fire, meaning that the initial mass loss includes the burning of liquid fuel, but this would not affect the peak burning flux. Results show that the flame could not sustain on the 5cm wood cribs with eight layers or 20cm wood cribs with less than two layers. However, when the flame can self-sustain, the peak mass flux is similar for wood cribs with the same layer numbers. Except for the 40-cm wood cribs, they always show a greater burning flux. When the wood crib size is constant at 20 cm, the mass loss flux increases with the layer numbers, as expected, because the fuel load density increases as the layer number of wood cribs increases. Many other parameters would affect the burning rate of wood cribs, such as the porosity, dimension, ignition, and so on. The current study focuses on the scale effect on the horizontal direction. Thus, only the data for wood cribs with the same layer number (eiight layers) and the varied horizontal scale are further analyzed.

The HRRPUA shown in Fig. 5 is calculated using the mass flux times the effective heat of combustion of material, where the effective heat of combustion for PMMA, propanol, and wood is 24.2 kJg^{-1} [9], 33.4 kJg^{-1} [31], and 18 kJg^{-1} [32] separately. The comparison of HRRPUA for different fuels in varied scales will be discussed in "Heat release rate per unit area" section.

Scale dependence of burning rate

Figure 6 summarizes the peak mass flux in different fuel sizes and types. The mass flux trends are distinct among fuel types. The burning of propanol pool fire displays a typical pattern, where the burning rate decreases first and then increases with the pool diameter. Similarly, the PMMA burning flux also decreases with the fuel size but becomes relatively constant when the fuel size exceeds 15 cm.

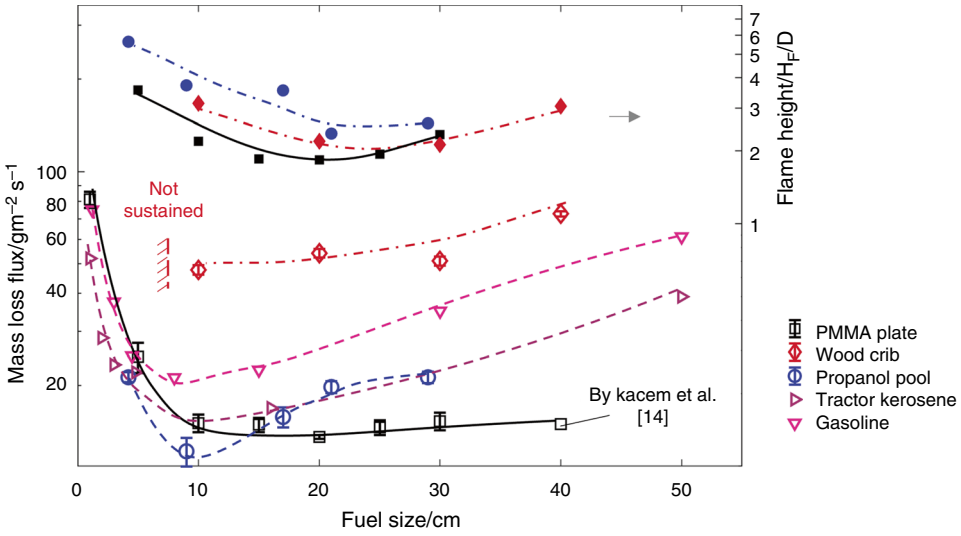

Fig. 6 Scale dependence of mass flux and flame height on fuel sizes

On the other hand, the burning of wood cribs presents a unique trend. If the mass flux is below the critical value, the flame is unable to sustain within the wood cribs. This is likely due to the strong cooling effect of small-size wood cribs in terms of the larger surface-to-volume ratio (Table 1). When the flame can be sustained, the mass flux remains constant first and then increases with the crib size. From the perspective of convective heat transfer and oxygen supply, the gap between the wood strips allows the air entrainment, flame spread and persistence within the cribs. Therefore, porosity is an important parameter in determining the burning rate. As listed in Table 1, the porosities are very close for the wood cribs with the same layer number (0.030–0.033). That could be one reason to explain why the wood cribs show a similar burning flux (~ 50 gm^{-2} s^{-1}) for different scales. However, as the wood crib size becomes large, the intensity of internal radiation feedback among wood strip increases accordingly and enhances the burning flux, leading to an increase in the burning flux, as shown in Fig. 6.

The diagram in Fig. 7 illustrates the physics of burning liquid and solid fuels on small and large scales. The sidewall heating has a significant effect on the burning rate for both types of fires. For small liquid fire, conduction and convection are dominant factors [33]. As the fuel size increases, both the burning and heat fluxes from the sidewall decrease, so the enhancement to the burning flux becomes small and even negligible 34. In larger-scale fires, flame radiation dominates the burning process, so the burning rate increases with the fuel size. Similarly, the burning of PMMA is also influenced by the sidewall flame heating, where the edge boundary is heated vigorously by the attached flame. The conductive heat transfer is reduced with the increasing fuel size. That is the reason that horizontal regression is more obvious in burning small-size ($D < 10$ cm) PMMA plate (Fig. 3a). In large PMMA fire, flame radiation is the dominant factor, so the fuel mainly regresses vertically (Fig. 3b). Table 2 summarizes the dominating factors in different fire scales for three fuel types.

Heat release rate per unit area

The diagram in Fig. 8 shows the calculation of the heat release rate per unit area (HRRPUA) based on mass flux and heat of combustion. Note that the data for tractor kerosene and gasoline are sourced from the literatures [21]. For liquid fuels, gasoline and kerosene have higher HRRPUA due to their high heat of combustion values. Propanol and PMMA have similar HRRPUA when the fuel size is less than 20 cm. However, the HRRPUA for propanol pool fire increases dramatically, approaching that of other liquid fuels. PMMA consistently has the lowest HRRPUA, even when the fuel size is increased. Wood cribs tested in this study have a similar HRRPUA with gasoline and kerosene when the size is smaller than 20 cm. Higher HRRPUA for larger wood cribs has been observed as the result of the positive heating feedback loop inside the wood cribs. These results are meaningful in analyzing the firepower of different fuels or judging equivalency for different fuels in terms of fire powers. For example, when simulating solid fuel with liquid fuel at the same firepower, a 10cm gasoline pool fire can serve as an equivalent 10cm wood crib fire. Similarly, a 10cm PMMA fire is more comparable to a propanol fire at the same size.

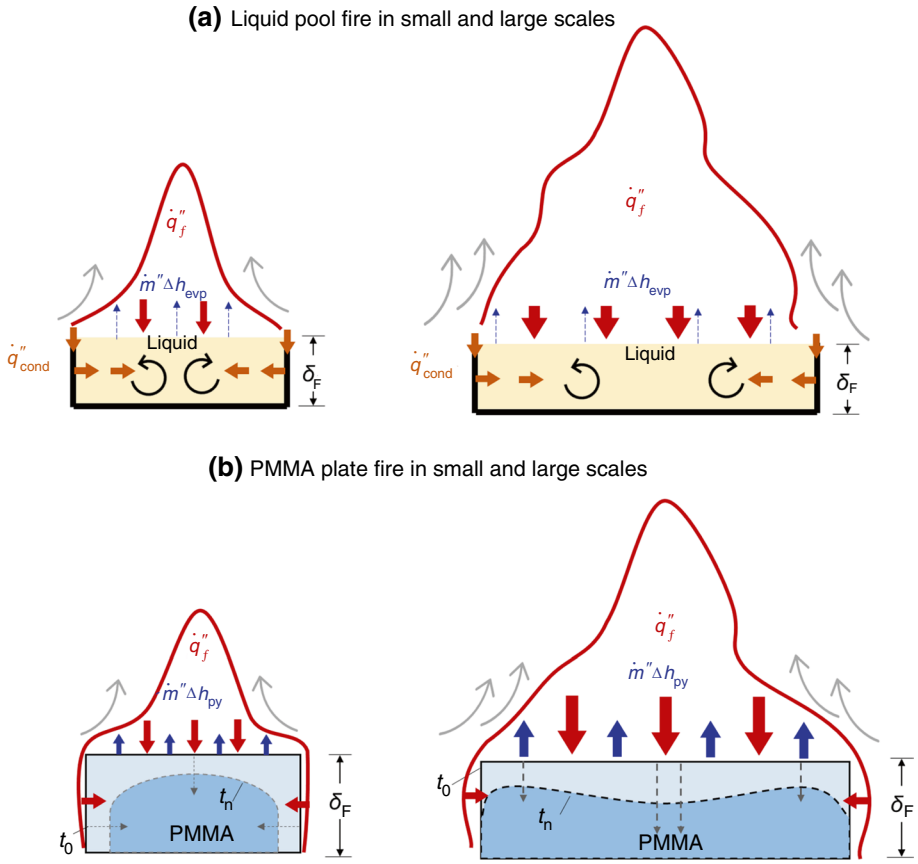

Fig. 7 Physics of **a** liquid pool fire and **b** solid PMMA fire

Table 2 Major influence factors at different fuel scales

	Liquid	PMMA plate	Wood crib
Small scale $D < D_c$	Wall conduction	Sidewall burning	Large cooling
Large scale $D > D_c$	Flame radiation	Flame radiation	Large internal radiation

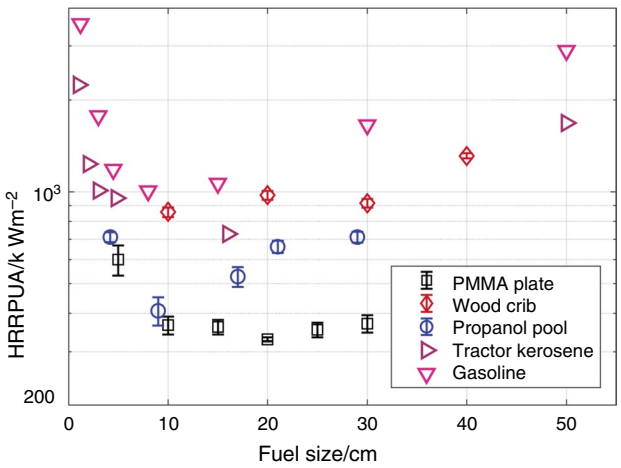

Fig. 8 The HRRPUA for representative liquid and solid fuels

Flame height

Flame height is one of the most important parameters to characterize a fire, as it visually reflects the fire size and is useful in fire protection engineering design. Thomas et al. [35] found that the flame height, which is defined as the distance between the flame tip to the top surface of the fuel bed (fuel bed height is ignored), can be well correlated with the fuel size and fire heat release rate. A closed-form equation to evaluate the flame height is given in Eq. (1) [21]:

$$l = 0.23\dot{Q}^{2/5} - 1.02D \tag{1}$$

where l is the flame height in m and is defined as the top of the flame body to the fuel bed surface. For wood crib fire, the fuel bed surface is selected as the topmost layer of wood.

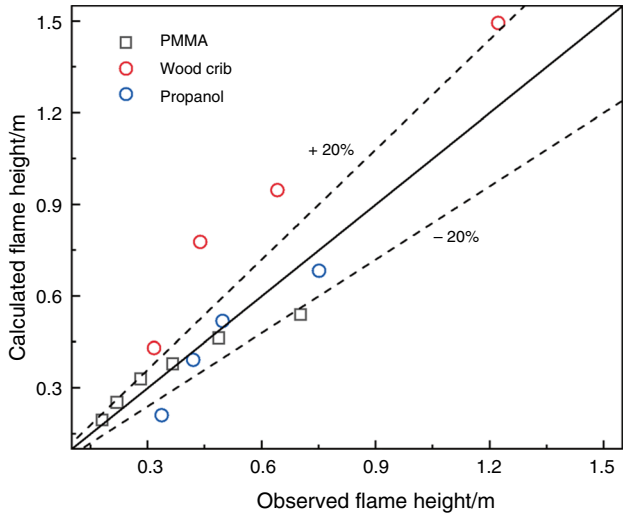

Fig. 9 The comparison between observed flame height with calculated flame height with Eq. (1)

$\dot{Q}$ is the heat release rate in kW, and D is the fuel bed diameter in m. It should be pointed out that the above equation is only valid in certain conditions. A detailed validity process is presented in Appendix A.

The flame height for PMMA, propanol pool fire, and wood crib with various dimensions is shown in Fig. 9. When increasing the fuel size, the fire heat release rate and flame height increase accordingly. It can also be observed that the liquid pool fire and PMMA plate show a good agreement between the observed flame height and calculated value (most points are within the region of ±20% error line in Fig. 9). However, the measured flame height of the wood crib is all smaller than the estimation based on the empirical equation. A possible reason is that the fuel was assumed to be an ideal plate when estimating the virtual source in Eq. (1), i.e., the thickness of the fuel bed was not taken into consideration. This assumption is suitable for the thin PMMA plate and the liquid pool, whose thickness is 2 cm and relatively small compared with the level of flame height (less than 10%). But for the wood crib, the fuel bed height is 20 cm, which is relatively large compared with the flame height. A large error will be caused when applying the virtual source assumption directly.

On the other hand, the special hollow structures of wood cribs enable the flame to be established not only at the top surface but also at the gaps between wood strips along the vertical direction. Therefore, simplifying the 3D volume combustion as a 2D surface reaction at the top surface may lead to the underestimation of the observed flame height. Overall, the comparison between three fuels also shows that the accuracy of the classical empirical is highly affected by the fuel bed geometry, whereas the fuel type (solid or liquid) has a relatively weak impact.

Equation (1) can be converted to the dimensionless format by dividing the fuel size D at both sides of the equal sign:

$$L^* = l/D = 0.23\left(\dot{Q}/D^{5/2}\right)^{2/5} - 1.02 \quad (2)$$

The dimensionless flame height with different materials and fuel sizes is further presented in Fig. 6. As shown, for all the studied fuel types, the dimensionless flame height decreases gradually with the increase in fuel size and almost keeps constant when the fuel size continues to grow. For example, the dimensionless flame height of PMMA decreases from 3.6 to 1.8 when the length of the PMMA plate increases from 5 to 15 cm, with around 50% of decay rate. However, as the PMMA plate size grows to 30 cm, the dimensionless flame height only increases to 2.2. The increase rate is around 20%, which is much smaller than the decay. This trend reveals the fact that the flame height is highly affected by the fuel size at a small scale. The larger fuel size increases the burning area, whereas the HRRPUA decreases rapidly (Fig. 8), leading to a decrease in the dimensionless flame height, while for large-scale ones, the constant dimensionless flame height represents that the flame height increases linearly with the fuel size, which could be well explained by the constant HRRPUA at the large fuel size regime.

Validation in numerical simulation

To further validate and test the results of this work, a set of numerical simulations are conducted with fire dynamics simulator (FDS). The numerical model consists of a $4\times4\times4$ m^3 cubic space, with a solid boundary at the bottom surface, and an open surface for the top surface and the rest four surfaces. A square fire source is set at the center of the bottom surface. The side length of the fire source varies from 5 to 100 cm. The HRRPUAs for different cases are valued by referring to the PMMA test results. In the numerical simulation, turbulence is modeled with the large eddy simulation (LES) model. The mixture fraction combustion model and the finite volume method are adopted for simulating the combustion process and radiation, respectively. The total simulation time is set as 200 s with a time step of 0.25 s.

To compromise the balance between the computational time and calculation resolution, a hybrid mesh system is adopted in the numerical tunnel, i.e., coarser mesh regions for the far-fire fields and one refined mesh region for the near-fire region ($1\times1\times1$ m^3) to make sure at least five grids are set for each length of the fire source. For the coarser mesh regions, a prior mesh independence study is conducted with the 30-cm fuel case. Compared with the flame height

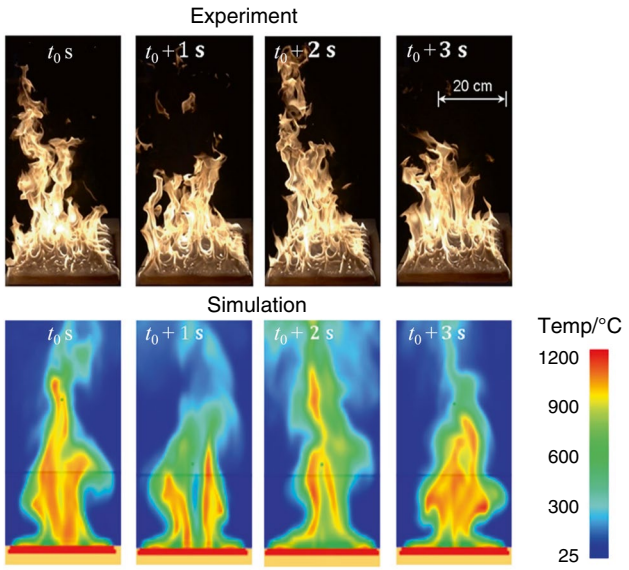

Fig. 10 Experiment versus numerical flame behaviors, where the fuel size is set as 30 cm

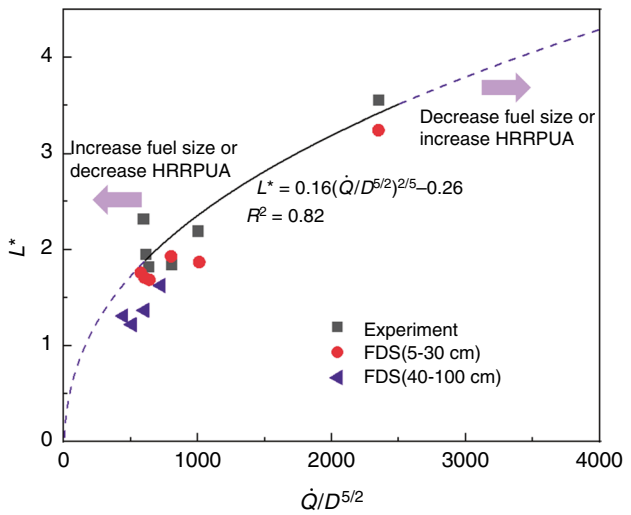

Fig. 11 Comparison with numerical results and extension of the fitting equation

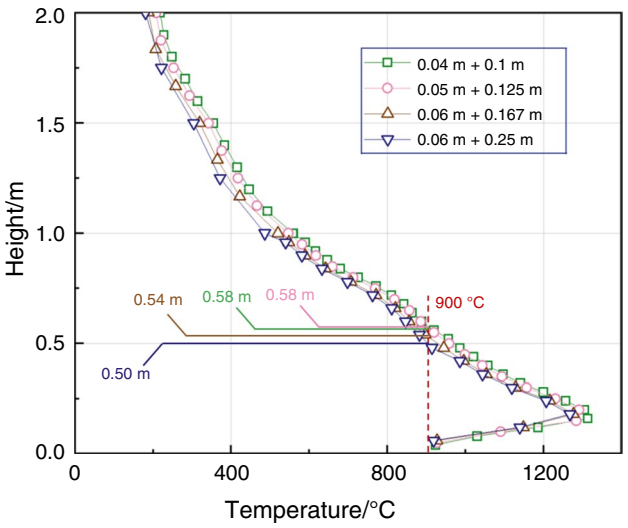

Fig. 12 Temperature distribution with different mesh systems, where the fuel is the 30-cm PMMA

results of 10 grid/m (0.1 m grid size), the relative error of flame height for mesh systems with 4, 6, and 8 grid/m are − 12.4%, − 6.6%, and 0.34%, respectively. Therefore, the mesh system of 8 grid/m (0.125 m + 0.05 m for the near-fire domain) was selected considering the accuracy and computational time. More detailed information about the mesh independence study is presented in Appendix B.

The simulated flame and the experimental phenomena with different fuel sizes are compared in Fig. 10. As shown, the flame geometry and structure, including the continuous flame region and intermittent flame region, can be well simulated in the numerical model. Moreover, the fluctuation of the flame caused by the turbulent combustion process can also be well observed in the numerical results with a similar frequency, indicating that the major flame characteristics have been solved numerically in an accurate way.

Based on the structure of Eq. (2), a new equation was fitted to better correlate with the results in the current study with R-squared value that equals 0.82:

$$L^* = l/D = 0.16\left(\dot{Q}/D^{5/2}\right)^{2/5} - 0.26 \tag{3}$$

Then, Eq. (3) is compared with the experimental data and numerical results in Fig. 11. Note that 900 ℃ isotherm is selected as the flame boundary in the numerical results [36]. As shown, within the experimental condition range, i.e., fuel size of 5–30 cm, the dimensionless flame height varies from 1.7 to 3.4. The proposed Eq. (3) agrees with both the experimental data and numerical results, which well validates the numerical results. When the fuel size in the numerical model continues to grow (40–100 cm group), L^* decreases accordingly. The extension of the fitted curve still well correlates with the flame height data beyond the experimental condition. The good agreement proves that the experimental data are solid and fitted equation has a good prediction capability for a large range of fuel sizes. The extension of Eq. (3) can be utilized in fire engineering design to quickly estimate the flame height, determine whether the possible fire can lead to a ceiling jet, and guide the installation of fire-detection and sprinkler systems.

Conclusions

In this study, a series of burning experiments with different fuel types and sizes, i.e., PMMA plate (5–30 cm), wood crib (5–40 cm), and propanol (9–29 cm), are carried out to investigate the size effect on the burning rate and flame behaviors. Results show that the burning rate of PMMA plate and pool fire share a similar trend in small size ($D < 10$ cm): With the increase in fuel size, the burning rate decreases. Analysis shows that for a small-scale fire ($D < 10$ cm), the sidewall burning largely contributes to the burning rate for the PMMA plate, while the pool fire burning is dominated by boundary heat conduction and internal convection. The sidewall heating decreases with the fuel size, resulting in a reduced burning rate. For wood cribs, small-scale fire ($D = 5$ cm) cannot be sustained due to the large cooling effect. With the increase in fuel size, the burning rate first keeps constant since the porosities (0.030–0.033) are close for the wood crib with 10–30 cm side length and then gradually increases under the effect of internal radiation when the side length is 40 cm.

Finally, the flame height with different test conditions is analyzed and compared with the classical equation. A new correlation of flame height with the fire heat release rate and fuel size is proposed, and its prediction capability is validated. This study quantifies the scale effect on the burning rate for the plate and crib solid fuel and provides experimental and theoretical support for understanding the fundamental burning phenomena.

Appendix

A: Validity of scaling flame height

The scaling analysis equation for flame height calculation is valid for certain conditions , as listed below []:

(1) Solid and liquid fuels are adopted in the experiment. When solid fuel burns, the surface undergoes thermal decomposition and produces combustible gases (vaporization at the surface for liquid fuel). These fuel gases escape at high temperatures and mix with the surrounding air's oxygen to form a flame. Since the combustible gases generated from the burning surface have relatively low flow velocities, the flow characteristics are primarily governed by buoyancy. The characteristic of buoyancy-driven diffusion flames is set by the release of fuel at low speeds, which aligns with the conditions observed during the solid/liquid fuel combustion in the present tests.

(2) The burner sizes in existing work range from 0.10 to 0.50 m. The fuel sizes in the present tests are well within this range.

(3) The characteristic HRR $\left(\dot{Q}/D^{5/2}\right)$ of the present experiments ranges from 600 to 2400 kW $m^{-5/2}$, which is consistent with the previously reported range of 600 to 40000 kW $m^{-5/2}$.

Therefore, using the scaling analysis of Eq. (1) to estimate flame height in the present work is reasonable and valid.

B: Numerical accuracy

The mesh independence of the numerical modelling was conducted by comparing the plume temperature distribution at the center axis of the 30-cm PMMA flame using different grid resolutions. Four different grid systems were considered: (a) 0.04 m + 0.1 m, (2) 0.05 m + 0.125 m, (3) 0.06 m + 0.167 m, (4) 0.06 m + 0.25 m. For these grid size combinations, the finer grid size was used for the near fire domain (1 m^3 space) and the coarser grid was adopted in the rest of the computation domain.

The average plume temperature from 100 to 200 s of different mesh systems is presented in Fig. 12. As shown, the temperature profile when using the combination grid of 0.05 m + 0.125 m are close to the modeling result with a finer grid (0.04 m + 0.1 m), indicating the grid quality is good enough to simulate the flame behavior. Meanwhile, by setting the threshold of 900 ℃, the flame height values for different grid systems are determined to be 0.58 m, 0.58 m, 0.54 m, and 0.50 m. Take the finest grid system as a reference, the relative errors are 0.34% (round-off error), -6.6%, and -12.4%, respectively. Therefore, the grid combination of 0.125 m + 0.05 m was selected considering the accuracy and computational time.

Acknowledgements This work is funded by the Hong Kong Research Grants Council Theme-based Research Scheme (T22-505/19-N). TZ thanks the support from the Hong Kong PhD Fellowship Scheme.

Funding Open access funding provided by The Hong Kong Polytechnic University.

Declarations

Conflict of interest We declare that this article is original, and it has been written by the stated authors and approved for its submission. This article has not been published previously and is not under consideration for publication elsewhere. All authors certify that they have no affiliations with or involvement in any organization or entity with any financial interest or non-financial interest in the subject matter or materials discussed in this manuscript.

Open Access This article is licensed under a Creative Commons Attribution 4.0 International License, which permits use, sharing, adaptation, distribution and reproduction in any medium or format, as long

as you give appropriate credit to the original author(s) and the source, provide a link to the Creative Commons licence, and indicate if changes were made. The images or other third party material in this article are included in the article's Creative Commons licence, unless indicated otherwise in a credit line to the material. If material is not included in the article's Creative Commons licence and your intended use is not permitted by statutory regulation or exceeds the permitted use, you will need to obtain permission directly from the copyright holder. To view a copy of this licence, visit http://creativecommons.org/licenses/by/4.0/.

References

1. Quintiere JG. Principles of fire behavior. 2nd ed. Boca Raton: CRC Press; 2016. https://doi.org/10.1201/9781315369655.
2. Lei J, Liu N, Zhang L, Deng Z, Akafuah NK, Li T, Saito K, Satoh K. Burning rates of liquid fuels in fire whirls. Combust Flame. 2012;159:2104–14. https://doi.org/10.1016/j.combustflame.2012.01.019.
3. Pizzo Y, Consalvi JL, Querre P, Coutin M, Audouin L, Porterie B, Torero JL. Experimental observations on the steady-state burning rate of a vertically oriented PMMA slab. Combust Flame. 2008;152:451–60. https://doi.org/10.1016/j.combustflame.2007.06.020.
4. Sibulkjn M, Lee CK. Flame propagation measurements and energy feedback analysis for burning cylinders. Combust Sci Technol. 1974;9:137–47. https://doi.org/10.1080/00102207408960349.
5. Chen Y, Fang J, Zhang X, Miao Y, Lin Y, Tu R, Hu L. Pool fire dynamics: principles, models and recent advances. Prog Energy Combust Sci. 2023;95:101070. https://doi.org/10.1016/j.pecs.2022.101070.
6. Chatris JM, Quintela J, Folch J, Planas E, Arnaldos J, Casal J. Experimental study of burning rate in jet-fuel pool fires. Combust Flame. 2001;126:1373–83.
7. Liu J, He Y, Zhou Z, Yao W, Yuen R, Wang J. The burning behaviors of pool fire flames under low pressure. FIRE Mater. 2016;40:318–34. https://doi.org/10.1002/fam.2289.
8. Quintiere JG. A semi-quantitative model for the burning rate of solid materials. National Institute of Standards and Technology, Building and Fire Research Laboratory; 1992 Jun 1.
9. Luche J, Rogaume T, Richard F, Guillaume E. Characterization of thermal properties and analysis of combustion behavior of PMMA in a cone calorimeter. Fire Saf J. 2011;46:451–61. https://doi.org/10.1016/j.firesaf.2011.07.005.
10. Smith PG, Thomas PH. The rate of burning of wood cribs. Fire Technol. 1970;6:29–38. https://doi.org/10.1007/BF02588857.
11. Heskestad C. Modeling of enclosure fires. In: Symposium (International) on combustion. 1973; 14:1021-1030. https://doi.org/10.1016/S0082-0784(73)80092-X
12. Zhang T, Wang Z, Wong HY, Tam WC, Huang X, Xiao F. Real-time forecast of compartment fire and flashover based on deep learning. Fire Saf J. 2022;130:103579. https://doi.org/10.1016/j.firesaf.2022.103579.
13. Carvel ROU, Beard AN, Jowitt PW. The influence of longitudinal ventilation systems on fires in tunnels. Tunn Undergr Sp Technol. 2001;16:3–21.
14. Pantousa D. Numerical study on thermal buckling of empty thin-walled steel tanks under multiple pool-fire scenarios. Thin-Walled Struct. 2018;131:577–94.
15. Blinov VI, Khudiakov GN. Diffusion burning of liquids. Carolina: U.S Army Enginner Research and Development Laboratories; 1961.
16. Evans DD, Walton WD, Baum HR, Notarianni KA, Lawson JR, Tang HC, Keydel KR, Rehm RG, Madrzykowski D, Zile RH. In-situ burning of oil spills: mesoscale experiments. 1992.
17. P. Sun, X. Huang, C. Xu (2022) Flashpoint and Burning of Thin Molten Plastic Pool Above Hot Boundary, Applied Thermal Engineering, 118931. https://doi.org/10.1016/j.applthermaleng.2022.118931
18. Apte VB, Green AR, Kent JH. Pool fire plume flow in a large-scale wind tunnel. Fire Saf Sci. 2006;3:425–34.
19. P. Sun, X. Zhang, C. Ding, X. Huang (2021) Effect of Reduced Pressure on the Burning Dynamics of Fire Whirl, Fire Safety Journal, 103419. https://doi.org/10.1016/j.firesaf.2021.103419
20. Hu L. A review of physics and correlations of pool fire behaviour in wind and future challenges. Fire Saf J. 2017;91:41–55. https://doi.org/10.1016/j.firesaf.2017.05.008
21. Drysdale D. An introduction to fire dynamics. 3rd ed. Chichester: Wiley; 2011. https://doi.org/10.1002/9781119975465.
22. Gollner MJ, Huang X, Cobian J, Rangwala AS, Williams FA. Experimental study of upward flame spread of an inclined fuel surface. Proc Combust Inst. 2013;34:2531–8. https://doi.org/10.1016/j.proci.2012.06.063.
23. N. Zhu, X. Huang, J. Fang, L. Yang, L. Hu (2021) Transitional flame-spread and fuel-regression behaviors under the change of concurrent wind, Fire Safety Journal, 103015. https://doi.org/10.1016/j.firesaf.2020.103015
24. Steckler K, Kashiwagi T, Baum H, Kanemaru K. Analytical model for transient gasification of noncharring thermoplastic materials. Fire Saf Sci. 1991;3:895–904. https://doi.org/10.3801/iafss.fss.3-895.
25. Modak AT, Croce PA. Plastic pool fires. Combust Flame. 1977;30:251–65. https://doi.org/10.1016/0010-2180(77)90074-8.
26. Kacem A, Mense M, Pizzo Y, Boyer G, Suard S, Boulet P, Parent G, Porterie B. A fully coupled fluid/solid model for open air combustion of horizontally-oriented PMMA samples. Combust Flame. 2016;170:135–47. https://doi.org/10.1016/j.combustflame.2016.04.009.
27. Folke F. Experiments in fire extinguishment, NFPA Q. 31. 1937.
28. Gross D. Experiments on the burning of cross piles of wood. J Res. 1962;66:99.
29. Hurley MJ. SFPE handbook of fire protection engineering. New York: Springer; 2015.
30. Zukoski EE. Fluid dynamic aspects of room fires. Fire Saf Sci. 1986;1:1–30.
31. Gong J, Zhang S, Cheng Y, Huang Z, Tang C, Zhang J. A comparative study of n-propanol, propanal, acetone, and propane combustion in laminar flames. Proc Combust Inst. 2015;35:795–801. https://doi.org/10.1016/j.proci.2014.05.066.
32. Ohmiya Y, Kang S, Noaki M, Delichatsios MA. Effects of opening aspect ratio on facade gas temperatures with and without sidewalls for underventilated conditions. Fire Saf J. 2020;113:102944. https://doi.org/10.1016/j.firesaf.2019.102944.
33. Babrauskas V. Estimating large pool fire burning rates. J Hazard Mater. 1983;19:251–61. https://doi.org/10.1007/BF02380810.
34. C. Xiong, Z. Wang, X. Huang, Modelling flame-to-fuel heat transfer by deep learning and fire images, Engineering Applications of Computational Fluid Mechanics. 2024;18:2331114. https://doi.org/10.1080/19942060.2024.2331114
35. Thomas PH, Webster C, Raftery M. Some experiments on buoyant diffusion flames. Combust Flame. 1961;5:359–67.
36. Prikhod'Ko NG, Lesbaev BT, Auelkhankyzy M, Mansurov ZA. Synthesis of graphene films in a flame. Russ J Phys Chem B. 2014;8:61–4.

Publisher's Note Springer Nature remains neutral with regard to jurisdictional claims in published maps and institutional affiliations.